Monthly Notices
of the
ROYAL ASTRONOMICAL SOCIETY
MNRAS **462,** 4464–4472 (2016) doi:10.1093/mnras/stw1839

Night-sky brightness and extinction at Mt Shatdzhatmaz

V. Kornilov,★ M. Kornilov, O. Voziakova, N. Shatsky, B. Safonov, I. Gorbunov, S. Potanin, D. Cheryasov and V. Senik

Lomonosov Moscow State University, Sternberg Astronomical Institute, Universitetsky pr-t, 13, 119234 Moscow, Russia

Accepted 2016 July 25. Received 2016 June 26; in original form 2016 April 5

ABSTRACT

The photometric sky quality of Mt Shatdzhatmaz, the site of the Sternberg Astronomical Institute Caucasian Observatory 2.5-m telescope, is characterized here by the statistics of the night-time sky brightness and extinction. The data were obtained as a by-product of atmospheric optical turbulence measurements with the MASS (Multi-Aperture Scintillation Sensor) device conducted in 2007–2013. The factors biasing night-sky brightness measurements are considered and a technique to reduce their impact on the statistics is proposed. The single-band photometric estimations provided by MASS are easy to transform to the standard photometric bands. The median moonless night-sky brightness is 22.1, 21.1, 20.3 and 19.0 mag arcsec^{-2} for the *B*, *V*, *R* and *I* spectral bands, respectively. The median extinction coefficients for the same photometric bands are 0.28, 0.17, 0.13 and 0.09 mag. The best atmospheric transparency is observed in winter.

Key words: atmospheric effects – site testing – techniques: photometric.

1 INTRODUCTION

It is well known that the efficiency of classical ground-based astronomical observations (resolution and limiting magnitude) depends strongly on the atmospheric seeing (Bowen 1964), but other astroclimatic parameters also play an important role. An overall telescope productivity is proportional to the clear-sky fraction. Observations of a faint object depend strongly on the night-sky brightness, which includes a contribution from light pollution. The accuracy of photometric observations is determined by the temporal and spatial stability of the atmospheric extinction.

When Mt Shatdzhatmaz in North Caucasus was chosen for the new 2.5-m telescope, we initiated in 2007 a long-term monitoring of the atmospheric seeing and other astroclimatic parameters at this site, pursuing two main goals: first, to support the operation of the 2.5-m telescope, and, secondly, to gain a better understanding of the astroclimate of North Caucasus.

The first results of these measurements are presented in Kornilov et al. (2010) where the hardware and technique used are also described. The summary results of the optical turbulence studies of the 2007–2013 campaign are given in Kornilov et al. (2014). In this paper, we present the results of measurements of the photometric parameters, the night-sky brightness and the atmospheric extinction.

The night-sky background was measured during optical turbulence monitoring with the MASS (Multi-Aperture Scintillation Sensor) device (Kornilov et al. 2007) because it is required to properly calculate scintillation indices (Tokovinin et al. 2003; Tokovinin & Kornilov 2007). More than 30 000 such sky background estimates were obtained during the campaign.

Since MASS is essentially a fast high-precision photoelectric photometer, it also allows us to estimate atmospheric extinction. To this end, the optical turbulence programme was complemented by special extinction measurements in 2009.

The first results of these measurements are given by Voziakova (2012). More comprehensive atmospheric extinction data are presented in Section 3. In the same section, it is shown how to transform the extinction measured in the MASS spectral band to the standard *U*, *B*, *V*, *R* and *I* photometric system.

The statistics of sky background estimates are given in Section 4. They are transformed to the conventional units of stellar magnitude per square arcsec using the known magnitudes of the MASS programme stars and the atmospheric extinction.

The results presented in this paper allow us to characterize the Sternberg Astronomical Institute (SAI) observatory comprehensively, facilitating the optimum scheduling of the 2.5-m telescope. Monitoring of the astroclimatic parameters will help in operating the telescope in the most efficient way.

2 FACILITIES DESCRIPTION

2.1 Astroclimatic campaign of 2007–2013

The Caucasian Observatory of SAI is located close to the Mt Shatdzhatmaz summit (Russia, North Caucasus, Karachay-Cherkess Republic, about 20 km to the south from the city of Kislovodovsk). The summit altitude is 2127 m above sea level and the mountain belongs to Skalisty ridge. The ridge is parallel to the Main Caucasian ridge,

★ E-mail: victor@sai.msu.ru

which is 50 km to the south. The Skalisty ridge extends to the west and then turns to the north, forming the North Caucasus watershed divide.

The 2.5-m telescope is installed 40 m from the steep side of the mountain at an altitude of 2112 m above sea level. The dome coordinates are 43°44′10″ N, 42°40′03″ E. Smaller telescopes are to be mounted in 5-m towers along the ridge, to the north-east of the main telescope. The facilities and the observatory infrastructure are located at a distance of 400 m from the towers, in a flat area. The solar station of Pulkovo Observatory is located 700 m to the north-west.

The southern part of the sky is free from light sources, while the northern part is illuminated by the townships of the Caucasian Mineral Water region. The stratovolcano Mt Elbrus (altitude 5624 m) is located at a distance of 47 km south-south-west from the observatory.

There are other astronomical observatories in the region. The Special Astrophysical Observatory of the Russian Academy of Science is located 100 km to the west, at the northern spurs of the Main Caucasian ridge. The Terskol Astronomical Observatory is located on the slopes of Elbrus. Unlike the SAI observatory, both of these are located close to higher peaks.

The Automatic Site Monitor (ASM) was installed in summer 2007 on the top of Mt Shatdzhatmaz, 40 m to the south-west of the 2.5-m telescope. Optical turbulence measurements were carried out from 2007 October to 2013 June. The monitoring hardware and its operating principles have been described by us earlier (Kornilov et al. 2010); this publication focuses on the optical turbulence measurements with the combined MASS/DIMM device.

The following characteristics for the atmosphere over Mt Shatdzhatmaz were established during the 2007–2013 campaign (Kornilov et al. 2014):

(i) The median seeing β_0 is 0.96 arcsec and it is better than 0.74 arcsec for 25 per cent of the time. The most probable value for the seeing is 0.81 arcsec. The free atmosphere seeing (above 1 km) is 0.43 arcsec. The best seeing is observed in October–November, when the median seeing is ≈0.83 arcsec. The optical turbulence is strongest in March (1.34 arcsec).

(ii) The median isoplanatic angle is 2.07 arcsec, also typical for many observatories. Its maximal value of 2.50 arcsec is reached in October. The median atmospheric time constant τ_0 is 6.57 ms, increasing to 10 ms in autumn.

(iii) The clear-sky time (Kornilov et al. 2016) is equal to 1320 h yr^{-1} or 45 per cent of the astronomical night-time. The majority of the clear night-time (≈70 per cent) is concentrated in the period from the middle of September to the middle of March. The maximum fraction of clear sky amounts to ≈60 per cent in November.

2.2 Photometric properties of the MASS instrument

The combined MASS/DIMM device uses both amplitude and phase distortions of the light coming through the atmosphere from the point source to measure atmospheric optical turbulence. The instrument and methods are described in detail in the paper (Kornilov et al. 2007). Below we briefly recall some important issues relevant to this paper.

The MASS/DIMM instrument is designed for use with common amateur 25–30 cm telescopes, convenient in field astroclimatic campaigns. The light from the telescope is directed to the different channels of the instrument by the specially designed optical beam-splitter (segmentator). The segmentator divides the input pupil into different subapertures. The MASS channel has four similar detectors corresponding to the four input coaxial apertures: A, B, C and D. Their diameters range from 2 to 9 cm.

For photometry, the apertures areas (3, 6, 20 and 30 cm^2 for the A, B, C and D channels, respectively) are essential. R7400P photomultipliers with stable fast electronics are used to measure the light fluxes in photon-counting mode with a dead time of ≈20 ns. The dark count of these bialkali photomultipliers is only a few pulses per second under typical night-time ambient temperatures. In comparison, the mean dark night-sky background signal is about 200 pulses s^{-1} in channels C and D. The measurements are carried out with microexposures of 0.5–1 ms, and the statistical moments are calculated for the counts.

The spectral response of MASS is determined both by the detector response curve and by the optics transmission.[1] The latter is especially important in the blue part of the spectrum. The effective wavelength of the resulting photometric response ranges from ∼450 to ∼500 nm for different copies of MASS being used at various observatories over the world. The MASS spectral response should be thoroughly studied because it is required for the correct measurement of the turbulence vertical profile.

If the non-linearity of the photon counters is properly accounted for (Kornilov 2008, 2014), the MASS device allows precise photometry in the MASS photometric band for stars of 0–7 mag. The scintillation noise is the primary source of photometric errors for these bright stars. Because of this noise, the minimum exposure time needed to reach a precision of 0.001 mag can be as long as 100 s (Kornilov et al. 2012).

3 ATMOSPHERIC EXTINCTION

3.1 Observations

The optical turbulence measurement programme was modified in 2009 January by including special observations to fulfil two tasks. Equal-altitude stars were measured to obtain the stellar magnitudes of programme stars outside the atmosphere, to produce a catalogue of photometric standards in the MASS band. Different-altitude stars were observed to measure the atmospheric extinction coefficient with the classical photometric pair technique.

The first report on the atmospheric extinction above the observatory was given by Voziakova (2012). Since then, the number of photometric observations has grown considerably. The number of measurements of low-altitude standards [at airmasses $M(z)$ of 1.35–2.0] has grown to ≈2500. The number of observed equal-altitude pairs has also increased, the magnitudes of the photometric standards have been refined and the list has been extended to 33 objects.

Measurements of photometric standards were carried out every 1.5 h if the atmospheric transparency was stable within ∼0.02 mag over 10–15 min. Such conditions were interpreted as a photometric sky condition. A set of photometric measurements consists of two or three stars: an equal-altitude pair, an extinction pair or both. One photometric measurement cycle takes 10–15 min.

Usually, the sky background is measured for 10 s after each telescope pointing. The photometric standard measurement is carried out for 2 min in the same manner as the optical turbulence measurement. The precision for the flux estimation is limited by the scintillation noise, that is ∼0.01 mag at zenith in the C and D

[1] http://curl.sai.msu.ru/mass/download/doc/mass_spectral_band_eng.pdf

MASS channels for a 1-s exposure time. For a 2-min exposure, the precision is about 0.001 mag, which may degrade to 0.005 mag for low objects. The contribution of the photon noise is less than 2×10^{-4} for any star used.

The pair technique provides reliable results only under photometric conditions because it is based on the assumption that the extinction coefficient α is the same in the directions to both stars. The conditions are called photometric when the sky is absolutely clear and uniform. Moreover, the stars in the pair are required to have a substantial airmass difference ΔM. An instrumental constant R is expressed using the extinction coefficient α as follows:

$$R = m_* + \alpha M(z) + 1.086 \ln F_*(z), \quad (1)$$

where $F_*(z)$ is the measured star flux and m_* is the magnitude of the photometric standard.

The instrumental constant connects the entrance pupil illumination to the measured signal. It depends on the detector sensitivity and the transmission of the optics. Variations of the instrumental constant are caused by the behaviour of the MASS detector, the ambient temperature, the contamination of the optics and misalignment of the optics. Since all these factors do not change the quantity R between two sequential measurements, they do not affect the estimate of the extinction coefficient α. Here we use the counts in the C channel, considering that the D channel is more sensitive to misalignment and fogging.

To analyse the atmospheric extinction, we use the measurements obtained with the MASS/DIMM device number MD09. The device MD41 installed in 2013 January has a substantially different spectral response. The difference between these devices for 'red' stars ($B - V \approx 1.5$ mag) is up to 0.2 mag.

3.2 Extinction coefficient in the MASS photometric band

Uncertainties for the catalogue magnitudes m_* of the photometric standards may lead to errors of the extinction coefficient. In our case, the magnitudes are known with an accuracy of better than 0.01 mag (Voziakova 2012). The effects of the photometric bandwidth (the colour term) can be neglected because only 'white' stars ($B - V < 0.4$ mag) are used to measure the extinction coefficient. These errors, including the flux measurement error, are magnified by a factor $1/\Delta M$ when the extinction coefficient α is calculated.

We determined the minimum acceptable difference ΔM between the extinction stars by comparing the distributions for the extinction coefficient α as a function of this threshold. The shape of the distribution is almost constant as long as $\Delta M > 0.2$. Because the sample size decreases as the airmass threshold increases, the final threshold was chosen to be $\Delta M > 0.25$. Given this threshold, 1786 extinction coefficient estimates were obtained.

The extinction coefficient α may be verified using the instrumental constant R. We assume that the instrumental constant varies smoothly over time and that two consecutive measures are similar. However, random variations of R are introduced by fluctuations of the ambient temperature, uncertainties in the extinction coefficient and other measurement errors. The distribution of such random variations of R has a Gaussian shape with a standard deviation of 0.025 mag and wide tails extending to ± 0.1 mag.

The criterion for filtering outliers of the instrumental constant and the corresponding coefficient α estimates is formulated by requiring that any quantity R must be close to the median of its 11 nearest neighbours, to within ± 0.1 mag. About 7 per cent of all estimates, including obvious outliers, were excluded by this procedure. The cumulative distribution of the filtered extinction coefficients α is shown in Fig. 1 by the dashed line.

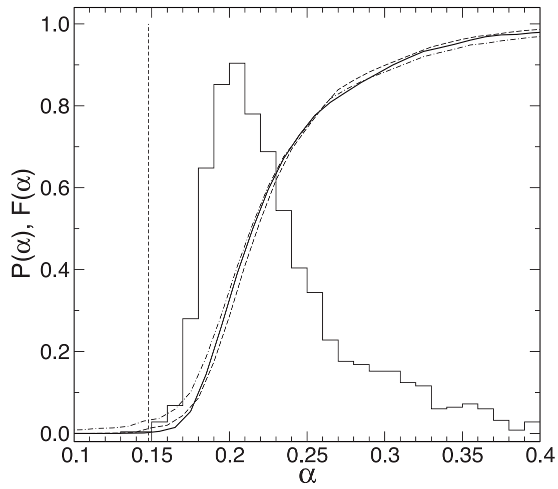

Figure 1. The probability density function of the final estimates of the extinction coefficient α in the MASS spectral band is plotted by the thin stepped line. The corresponding cumulative probability function is shown by the thick line. The dot-dashed line shows the distribution for the initial estimations. The dashed line is the distribution after filtering 7 per cent of the data. The vertical line denotes the extinction coefficient for a pure Rayleigh atmosphere.

Table 1. Quantiles of the extinction coefficient α for the MASS band and for the standard photometric bands, in magnitudes.

Photometric band	5%	25%	50%	75%	95%
MASS	0.17	0.19	0.22	0.25	0.34
U	0.46	0.49	0.51	0.55	0.67
B	0.23	0.25	0.28	0.31	0.42
V	0.13	0.15	0.17	0.20	0.28
R	0.10	0.11	0.13	0.16	0.23
I	0.06	0.08	0.09	0.11	0.17

On the other hand, one can estimate the extinction coefficient using the expression $\alpha M(z) = R - m_* - 1.086 \ln F_*$, based on the near-zenith star flux and the smoothed instrumental constant. The distribution for ≈11 000 samples obtained by this alternative formula is in agreement with the previous one. Such an approach is useful mostly for real-time monitoring of atmospheric transparency.

A combined, robust estimate of the extinction coefficient α can be obtained by averaging the results of the pair method and those of the alternative method based on the smoothed instrumental constant. It should be more reliable because it uses more information. Probably, a detailed error analysis would allow us to determine the optimal weights of such averaging, but here we use a purely empirical approach. The resulting distribution of the average α estimates becomes a little narrower than the initial one.

The probability density function and the corresponding cumulative distribution of α are shown in Fig. 1. One may see that the quantiles of the distribution are in good agreement, to within 0.01 mag, independently of the filtering approach. The most probably value is $\alpha = 0.20$ mag. In the figure, the Rayleigh atmosphere extinction coefficient calculated for the summit altitude by LIBRADTRAN (see Section 3.3) is plotted as a reference. The final distribution quantiles are given in Table 1.

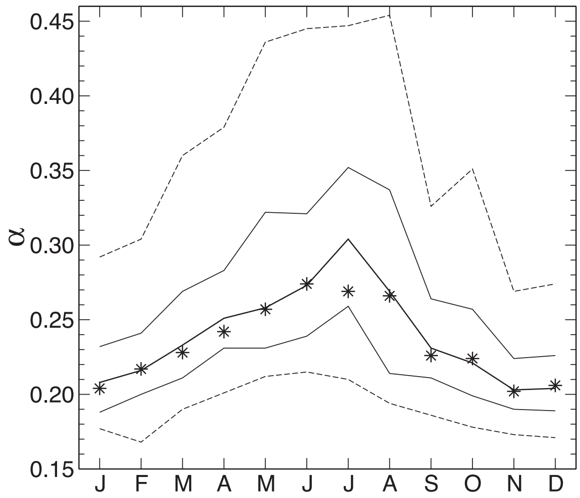

Figure 2. Variations of the quantiles of the extinction coefficient α over the year. The medians of the extinction measured by the pair method are plotted with asterisks. The thick solid line shows the medians for the *R*-based extinction estimates. The dashed lines show the 5 and 95 per cent marginal quantiles. The thin lines show the 25 and 75 per cent quantiles.

The annual variation of the extinction is shown in Fig. 2. The number of extinction measurements by the pair method is $\lesssim$100 during spring and summer months. This makes it impossible to determine the marginal quantiles reliably.

For this reason, for any near-zenith star measurement we use the extinction estimated from the smoothed instrumental constant. The quantiles for this sample are show in the figure. The median curves are in good agreement for all months except July. However, there is no doubt that the best transparency is observed in November–January and the worst is observed in June–August. The probability of a night with poor transparency (α > 0.4 mag) is considerably higher in the summer months.

3.3 Extinction in the standard photometric system

The MASS photometric band is located between the standard *V* and *B* bands, closer to the latter. For our device MD09, the effective wavelength is 479 nm for stars of spectral class A0 V. This spectral range is situated in the convenient part of the atmospheric transmission window where the extinction is determined only by the Rayleigh and aerosol scattering. Other atmospheric components (ozone and water) scarcely affect the extinction in the MASS band. However, their impact may be considerable in other photometric bands.

We use the package libRadtran (Mayer & Kylling 2005) to calculate the atmospheric transmission in the spectral range of 300–1200 nm. The atmospheric structure is defined by the standard mid-latitude atmosphere model from the paper (Shettle 1990). The aerosols are described by model number 1 from that paper. Their concentration is given by the specific input parameter 'visibility' measured in kilometres in libRadtran. The precipitable water vapour is specified as usual in millimetres. The ozone concentration is specified in Dobson units (100 DU = 1 mm).

The aerosol concentration obviously makes a major impact on the atmospheric extinction variance. The visibility parameter variation range for the simulation was chosen to cover the whole observed range of the MASS-band extinction. The precipitable water vapour amount was set to the median value 7.65 mm corresponding to the

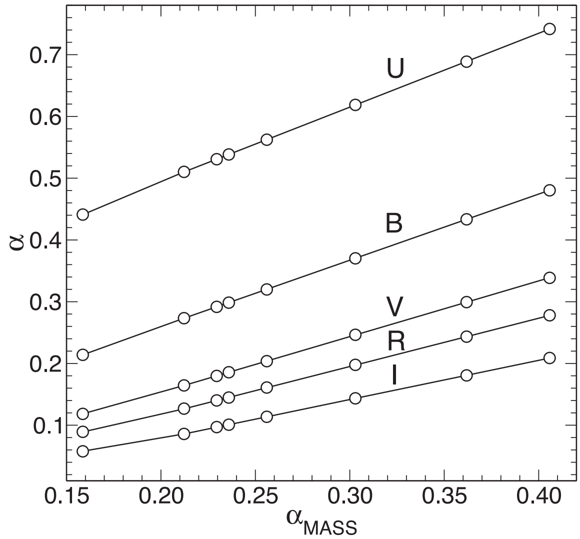

Figure 3. Calculated dependence of the extinction coefficients α (circles) for photometric bands *U*, *B*, *V*, *R* and *I* on the measured extinction coefficient for the MASS photometric band.

results of Voziakova (2012). The ozone concentration was determined by the Multi Sensor Re-analysis (MSR) data of the project Monitoring atmospheric composition and climate (van der A, Allaart & Eskes 2015).[2] The ozone concentration varies from 280 to 400 DU, and its median is 315 DU.

The spectral transmission curves obtained by the simulation with libRadtran were convolved with the source spectrum of α Lyr and the response curves for the bands *U*, *B*, *V*, *R*, *I* and MASS. The results are expressed as the extinction coefficient α as a function of the visibility parameter. Alternatively, they can be expressed as a function of the MASS-band extinction. The dependencies are shown in Fig. 3. Since they are almost linear, the extinction measured with the MASS instrument can be easily transformed to the extinction coefficient for any standard photometric band. A small deviation from linearity arises because of the bandwidth effects. It should be stressed that the dependencies are calculated for the spectral response of the specific MD09 device.

The extinction coefficient quantiles obtained by the described technique are given in Table 1. The transformation stability has been proven by varying the ozone and water vapour concentrations within their observed ranges. The precipitable water vapour was varied from 1 to 20 mm (see Kornilov et al. 2016), and the ozone was varied from 280 to 400 DU. The impact of ozone variation on the extinction coefficient is less than 0.005 mag. The precipitable water vapour variation affects mostly the bands *R* and *I*, where its impact attains 0.008 and 0.012 mag, respectively.

4 NIGHT-SKY BRIGHTNESS

4.1 Specifics of the sky brightness measurement with MASS

Recall that when the sky brightness is measured with photomultipliers, the contribution of faint stars is a major problem (Leinert et al. 1995; Mattila, Vaeisaenen & Appen-Schnur 1996; Krisciunas 1997) because a large field aperture (1–2 arcmin) has to be used to obtain statistically significant results. The only way to minimize the

[2] http://www.temis.nl/macc/index.php?link=o3_msr_intro.html

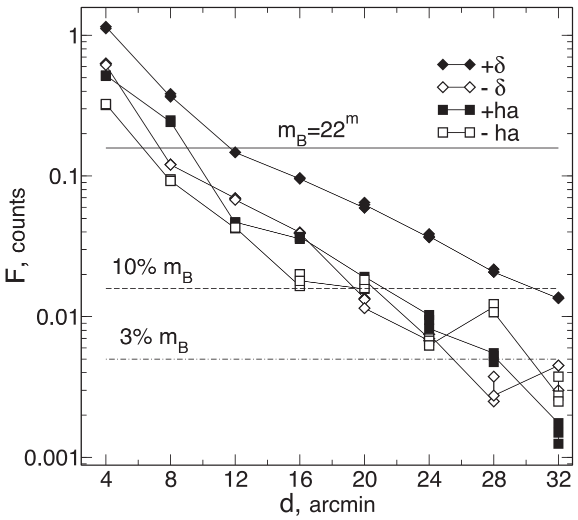

Figure 4. Scattered light (sum of the counts in the channels C and D), normalized to the α Lyr stellar magnitude, versus the distance from Sirius for four directions (see legend in the plot). The horizontal lines denote the dark night-sky brightness, and 10 and 3 per cent of it.

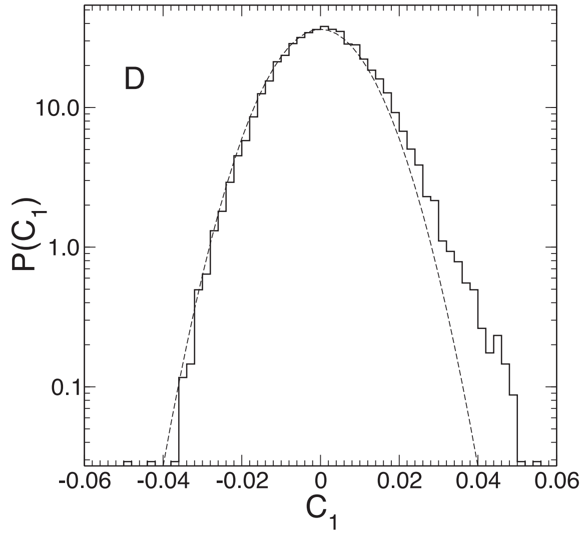

Figure 5. The stepwise curve is the distribution of C_1 for the overall set of 17 162 measurements in the D channel. The dashed line is the theoretical Gaussian distribution according to equation (2).

contamination was to choose a star-free sky patch intentionally. The MASS field aperture is even larger. Its angular diameter is about 4 arcmin and in our observations the fields were chosen randomly in the vicinity of bright programme stars because the task of night-sky brightness measurement was addressed only a posteriori.

Most observations were carried out with the MD09 device. Its aperture area is 39 800 arcsec^2 (0.003 deg^2). Given that the night-sky brightness is expected to be close to 22 mag arcsec^{-2}, the corresponding sky signal is equivalent to a star of 10.5 mag when such a large aperture is used. As follows from the probabilistic estimation based on the star density (Allen 1973), the mean overall star brightness in the MASS aperture is close to $\approx$11.4 mag and corresponds to an addition of $\sim$0.4 mag to the sky signal.

Scattered light from the bright programme stars is another effect leading to an overestimation of the sky background. The typical sky signal is $\sim 10^4$ times fainter than a programme star. The telescope mount randomly moves by 5 arcmin to measure the sky background, but it appears that the contribution of the scattered light remains considerable at such an angular distance. Actually, our preliminary analysis provides evidence for the statistical correlation between the sky brightness and the magnitude of a programme star.

Dedicated measurements of the background around Sirius (MASS magnitude is -1.5) were carried out in 2016 January. They show that the scattered light for α Lyr, the brightest programme star, is about $\sim$10 per cent of the signal from a dark sky at a distance of 20 arcmin. The scattered light depends not only on the magnitude, but also on the direction of the angular offset; it is larger for offsets towards the instrument's viewer (see $+\delta$ in Fig. 4). Indeed, the light of a star displaced from the optical axis by 30 arcmin is not fully blocked because of the telescope and instrument geometry.

As we pointed out before, the sky background was measured during the whole campaign, because it is required for the optical turbulence measurement. However, only the data obtained since the start of regular observations in 2008 March are used here to estimate the astronomical night-time sky brightness. After rejecting the outlying points, there are 17 162 measurements in total for any MASS channel, each mostly 10 s long or at least 9 s long.

4.2 Starlight and scattered light effects

Recording the background in MASS is done in the same way as the stellar scintillation measurement, and, hence, it contains a spatio-temporal correlation of the counts with a 1-ms resolution. The basic assumption for the following method of starlight estimation is that there is no atmospheric scintillation and no temporally correlated signal in the sky background flux.

Let us denote the temporal covariance of the flux F with a 1-ms lag by Cov$_1$[F]. This statistic is strictly zero for the sky background and close to the scintillation variance for the star flux. The covariance appears to be the most suitable diagnostic of scattered light because, unlike the variance, it does not need a precise evaluation of the Poisson noise contribution.

For the real data, the sample covariance c_1 is calculated instead of Cov$_1$[F]. Therefore, the statistic C_1, the ratio of c_1 to the sample mean, has a zero expectation and the following variance:

$$\mathrm{Var}[C_1] = \mathrm{Var}\left[\frac{c_1}{\bar{F}}\right] = \frac{1}{N}, \tag{2}$$

where N is the number of flux counts. For an exposure time of 10 s, $N \approx 10\,000$. The flux F is the number of registered pulses per 1 ms (counts).

When a correlated stellar signal F_* is present together with the background count F_{B}, the statistic C_1 increases and its expectation becomes

$$\mathrm{E}[C_1] = \frac{F_*^2\, s_1^2}{F_* + F_{\mathrm{B}}}, \tag{3}$$

where the covariance index s_1^2 is defined by the input aperture geometry and the atmospheric optical turbulence. On average, it is $\sim$0.02 for the C and D channels. It is clear that we can increase the effect by summing C_1 for two or more channels, using that the flux ratio of any two channels is a constant value.

Fig. 5 displays the empirical distribution of the statistic C_1 and its approximating normal distribution with a variance σ^2 calculated using expression (2). One can see the excess of positive values. Unfortunately, for our measurement parameters, the events with $C_1 > 3\sigma$ correspond to relatively bright stars that exceed the sky flux and occasionally ($\sim$3 per cent) appeared in the device aperture.

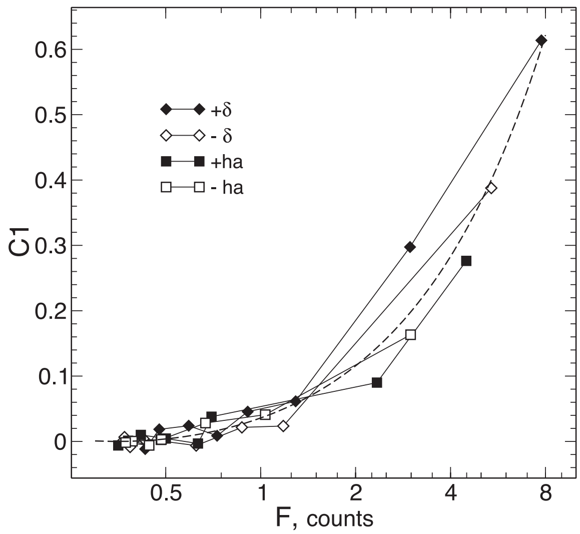

Figure 6. Dependence of the statistic C_1 on the flux in the D channel for scattered light from Sirius, in four offset directions. The dashed line denotes the approximation using equation (3).

Because of that, we statistically account for the stellar 'pollution' further. This correction is valid only statistically, rather than for the individual estimations.

The dependence of C_1 on the total signal in the field aperture (the sky background and the scattered light) obtained during measurement of the scattered light from Sirius is given in Fig. 6. This dependence agrees well with equation (3), whose prediction is shown by the dashed line for $s_1^2 \approx 0.08$ corresponding to the covariance observed at the time of the experiment. This way, we assume that the scattered light pollution is statistically equivalent to the faint star contribution. Below, both effects are considered jointly.

For the background data, the dependence of C_1 on the measured flux in the D aperture $\bar{F} = F_* + F_{\rm B}$ shows that the largest positive excess is observed near $\bar{F} \approx 1$. This is confirmed by the sub-sample medians, where each sub-sample is 1/10 of the full data set sorted in ascending order. The medians are plotted in the top panel of Fig. 7. Here, the combined C_1 parameter for the C and D channels is used. There is virtually no excess for faint fluxes, then it increases by $\sim$0.01, and then it decreases again. The impact of starlight helps to explain this dependence. Low values of $\bar{F} = F_* + F_{\rm B}$ are encountered only if the stellar light is much less than $F_{\rm B}$. For higher fluxes F_*, the measured points are shifted to the middle of the graph. The impact of the stellar flux on C_1 (equation 3) becomes unobservable for a high sky background $F_{\rm B}$.

The median stellar fluxes inducing the observed excesses are plotted in the bottom panel of Fig. 7. One can say that the flux F_* increases while $F_* < \bar{F}$ and then saturates at a constant level. The stellar flux fraction in the measured signal is significant and reaches a maximum of 0.4. Since this maximum is not located at the beginning, the minimal values of the measured sky background distribution are not distorted.

High-altitude clouds leading to small flux variations ($\sim$10 per cent) also affect the measured sky fluxes. The sky brightness usually increases considerably due to the light back-scattered by the Earth surface. For this reason, we consider separately the sky measurements carried out during photometric sky conditions. Their number is significantly less (4566) in spite of the fact that photometric conditions occur for $\sim$50 per cent of the clear time, because the sky background was rarely measured in stable conditions. The

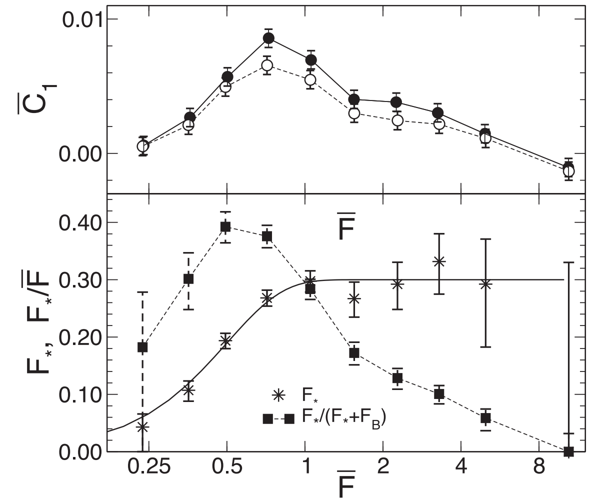

Figure 7. Top panel: 10 subsequent sub-sample medians for the full sample of 17 162 background estimates (filled circles) and after filtering the $\pm 3\sigma$ outliers (open circles). Bottom panel: Stellar flux F_* in counts (asterisks) and its impact on the total mean flux $\bar{F} = F_* + F_{\rm B}$ (filled squares) in the D aperture. The solid line shows the F_* approximation from equation (4).

behaviour of the median statistic $\bar{C}_1$ does not change for the selected clear-sky measurements. Moreover, the observed excess becomes a little larger.

Finally, we accept this estimate of stellar flux contribution (both faint stars and scattered light) in the measured sky background as reliable enough to be used for its correction. We use the approximation in the form

$$\bar{F}_* = 0.3\,(1 - \exp(-4\bar{F}^2)) \qquad (4)$$

and subtract this correction $\bar{F}_*$ from the flux $\bar{F}$ measured in channel D.

4.3 Night-sky brightness in the MASS photometric band

The night-sky brightness is conventionally expressed in magnitudes per square arcsec at zenith (Krisciunas 1997; Sánchez et al. 2007) because a considerable amount of the sky radiation is produced inside the Earth atmosphere. Given the instrumental constant R, the following simple expression is used to obtain the night-sky magnitude:

$$m_{\rm B}^{\circ}(z) = R - 1.086 \ln F_{\rm B}(z)\,. \qquad (5)$$

The smoothed instrumental constant was obtained in Section 3 for the full duration of the measurement campaign, except for the period starting in 2013 January with device MD41, and interpolated on to sky measurement moments. As a result, 11 580 night-sky brightness magnitudes were obtained, 4227 of which corresponded to photometric conditions.

Equation (5) provides the night-sky brightness $m_{\rm B}^{\circ}$ at a given sky point. One may use simple expressions from Garstang (1989) and Pedani (2014) to calculate the night-sky brightness at the zenith. Our measurements have been carried out at airmasses $M(z) < 1.3$ (except for a small fraction near the extinction standards). The median airmass is 1.09. The analysis shows that the correction to zenith is less than 0.02 mag and it is neglected here.

For measurements in moonless periods under photometric conditions, the sky magnitude $m_{\rm B}^{\circ}$ distribution quartiles are correspondingly 10.34, 10.00 and 9.32 mag. These values confirm the

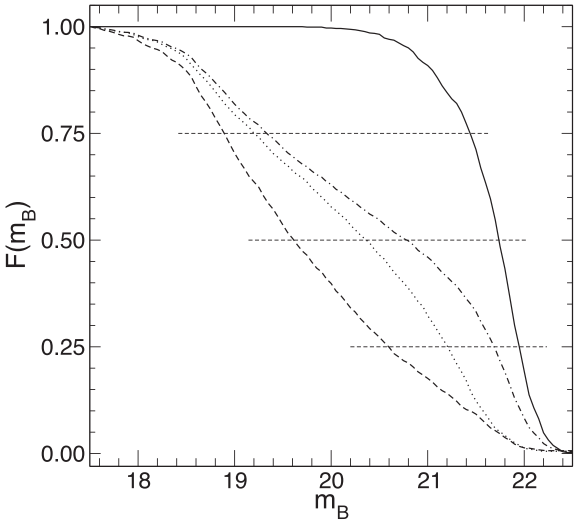

Figure 8. Night-sky brightness complementary cumulative distributions for photometric conditions in moonless periods (solid line), in moonlit periods (dashed line) and for all data (dot–dashed). The dotted line shows the complete distribution without stellar light correction. The horizontal lines mark the quartile levels.

preliminary estimate that stellar light may considerably impact the night-sky brightness measurements. To transform the sky brightness m_B to units of magnitude per square arcsec, the additional constant 11.50 mag, corresponding to the aperture area in arcseconds, should be added.

The empirical differential distribution of m_B is narrow enough (its width is less than 1 mag) under a moonless sky, i.e. when the Moon elevation is less than $-5°$. The most probable night-sky brightness is about 21.8 mag. The right bound of the distribution (the darkest sky) corresponds to 22.4 mag. A comparison between the distribution described above and the overall data distribution (with any sky quality data) shows that the latter has many more estimates brighter than 21 mag. This is explained by the additional light scattered by light clouds and fumuli. At the same time, some excess of dark sky due to additional extinction in clouds is observed.

The background measurements cover more than 5 yr. Initially, the nearest light pollution sources were located on the solar station, 800 m away. The local light pollution has changed dramatically since autumn 2011, when construction of an observatory began 40 m from the ASM. In the summer of 2012, a bright lamp was installed on the ASM tower to floodlight the construction area permanently.

To check the influence of local light pollution, we divided the moonless night-sky brightness measurements into five 1-yr seasons beginning July 1. Per season empirical cumulative distribution functions show that the first three seasons do not differ from each other and the 25 per cent quartile is equal to 22.0 mag. The season 2011/12 demonstrates a brightening by 0.2 mag. The sky brightness increased by another 0.5 mag in the season 2012/13. These seasons were excluded from the final statistics. Of course, light discipline has been recovered after installation of the telescope.

This night-sky brightening is unlikely related to the Solar activity maximum in 2013. The impact of Solar activity has been widely discussed by many authors (Krisciunas 1997; Patat 2003). However, let us note that the MASS spectral band (as well as the *B* band) are mostly free of night-sky emission lines.

Complementary cumulative distributions of the final samples are presented in Fig. 8 for different conditions. To estimate the impact of stellar light, the distributions of the sky brightness corrected with equation (4) and uncorrected are shown. The quartiles of these distributions are given in Table 2.

The interquartile range of the moonless night-sky brightness distribution is 0.51 mag or 1.6 times. The most probable brightness is 21.85 mag arcsec^{-2}.

Table 2. Quartiles of the night-sky brightness distribution in the MASS photometric band, expressed in units of magnitudes per square arcsec. The column *N* shows the sample size.

Sample	25%	50%	75%	*N*
Uncorrected	21.20	20.37	19.20	2439
Corrected	21.69	20.78	19.33	2439
Moon above horizon	20.59	19.62	18.89	1494
Moon below horizon	21.95	21.74	21.44	945

Table 3. Moonless night-sky colours. Values and standard deviations (STDs) are in units of magnitudes. *M* is the MASS band magnitude.

Colour	$B-M$	$M-V$	$B-V$	$V-R$	$V-I$
Value	0.37	0.66	1.03	0.77	2.10
STD	0.04	0.09	0.12	0.13	0.20

Table 4. Quartiles of the night-sky brightness distribution in photometric bands *B*, *V*, *R* and *I*. The values are in units of magnitude per square arcsec.

Photometric	Moon below horizon			Moon above horizon		
band	25%	50%	75%	25%	50%	75%
B	22.31	22.10	21.84	20.87	19.73	18.96
V	21.28	21.07	20.81	20.38	19.45	18.76
R	20.51	20.30	20.04	19.85	19.18	18.57
I	19.18	18.97	18.71	18.78	18.43	18.06

4.4 Night-sky brightness in the standard photometric system

The night-sky brightness can be transformed to the standard photometric spectral bands *B*, *V*, *R* and *I*. We use the spectra of the moonless night-time sky obtained using FORS1 (Patat 2008) at ESO Paranal Observatory in the decade to calculate the sky colours. These data are freely available on the web[3] and consist of hundreds of spectra in absolute energy units. The zero point is found using the α Lyr spectrum from Hayes (1985). The magnitudes of α Lyr are supposed to be 0.0 mag for all bands except MASS, where it is equal to 0.05 mag (Voziakova 2012). To obtain the $B-M$ and $M-V$ colours (where *M* is the MASS band magnitude), one needs to integrate the night-sky spectra with the corresponding reaction curves. The mean night-sky colours are given in Table 3.

Note that the calculated night-sky colours agree well with the previously published values in Patat (2003). Time-varying night-sky emission lines affect the magnitudes in bands *V*, *R* and *I*. The moonless night-sky brightness estimates in the standard photometric bands, obtained using the calculated colours, are given in Table 4.

To obtain the night-sky colours in the presence of the Moon, the numerical ESO model (Jones et al. 2013) was used. The model calculates the synthetic sky spectrum for a given phase angle, Moon

[3] http://www.eso.org/~fpatat/science/skybright/

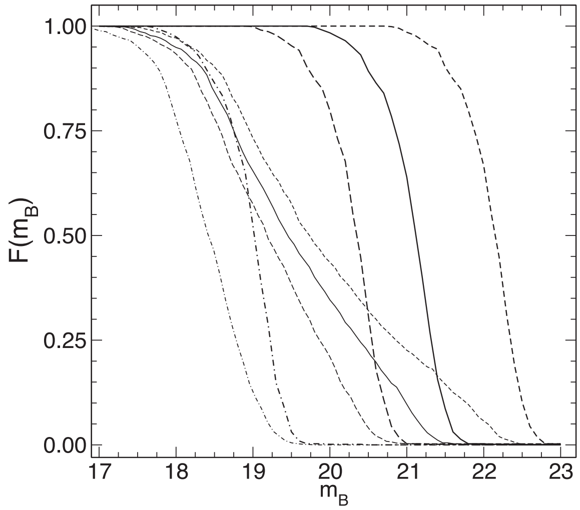

Figure 9. Complementary cumulative distribution of the night-sky brightness in different spectral bands: *B* (dashed), *V* (solid), *R* (long-dashed) and *I* (dot–dashed). The thick lines denote distributions for moonless periods, and the thin lines are the moonlit case.

elevation and Moon–target distance.[4] Using the synthetic spectra, we calculated the night-sky colours for the actual observing conditions and transformed our measurements to the standard photometric bands. The results are presented in Fig. 9 in the form of complementary cumulative distributions. The quartiles of these distributions are given in Table 4.

Recall that these statistics were calculated only on the data before autumn 2011, thus excluding the period of strong local light pollution. For the complete sample including the rejected data, the statistics change slowly, the quartiles becoming brighter by ∼0.1 mag in moonless periods. Under moonlight, the changes are less than a few ∼0.01 mag.

5 CONCLUSIONS

The above results illustrate that a slight modification of the optical turbulence measurement algorithm allows us to obtain additional information from MASS/DIMM measurements. The possibility of studying the photometric properties of the atmosphere with MASS/DIMM was pointed out by us a long time ago (Kornilov et al. 2007).

To determine the extinction in the MASS photometric band, the widely used method of pairs was adopted. Its ability to yield nearly instantaneous extinction estimates with minimum resources was fully employed. This method requires precise above-atmosphere instrumental magnitudes of the reference stars. At least a year-long cycle of measurements is needed to obtain a consistent solution of the respective system of photometric equations. The weather at Mt Shatdzhatmaz is such that a significant part of the observing time occurs on partially clear nights, when other methods of estimating the extinction are not feasible.

The transformation of the measured MASS band extinction coefficients into the standard *B*, *V*, *R* and *I* photometric system leads to the following median extinction values: 0.28, 0.17, 0.13 and 0.09 mag, respectively.

[4] https://www.eso.org/observing/etc/skycalc/skycalc.htm

Recall that a specific task to monitor the night-sky brightness was not initially planned and, as a result, the data presented in Section 4 suffer from uncertainty and incompleteness. In particular, the light scattering in the telescope and instrument that was not accounted for led to significant errors in the individual estimates of the sky brightness during moonless periods. Still, it was possible to derive reasonable statistical estimates of the night-sky background. When transformed into the standard photometric system, they are 22.1, 21.1, 20.3 and 19.0 mag arcsec^{-2} in the *B*, *V*, *R* and *I* bands, respectively.

The scattered light and star contamination are not important when measuring the sky background with the Moon above the horizon. However, building a consistent model of the Moon background at our site, similar to Jones et al. (2013), is not straightforward because it requires many input parameters and additional measurements.

Monitoring of the photometric atmospheric properties will definitely be continued. The background measurement algorithm has already been improved. Measurements are now performed at 27 arcmin offset from a programme star and in two positions. The extinction cycle now includes two low-altitude stars in different parts of the sky.

The emphasis for photometric measurements has now shifted to the real-time use of the data for flexible planning of observations, while achieving statistical completeness has a lower priority. Special programmes may acquire more time during optical turbulence monitoring and optimally will include feedback from observation schedulers working for the telescopes at this site.

ACKNOWLEDGEMENTS

The authors are sincerely grateful to the SAI scientific community, which welcomed our activity in astroclimatic research at Mt Shatdzhatmaz described in this and other papers. We would like to thank A. Tokovinin for valuable remarks on the content and structure of the current article. Considerable help for this work was given by P. Kortunov, A. Belinski and, during the last 2 yr, local observatory staff. As before, the support of solar station of Pulkovo Observatory, who opened the way to start the current research at the site, is acknowledged.

REFERENCES

Allen C. W., 1973, Astrophysical Quantities. Univ. London, Athlone Press, London

Bowen I. S., 1964, AJ, 69, 816

Garstang R. H., 1989, PASP, 101, 306

Hayes D. S., 1985, in Hayes D. S., Pasinetti L. E., Philip A. G. D., eds, Proc. IAU Symp. 111, Calibration of Fundamental Stellar Quantities. D. Reidel Publ. Co., Dordrecht, p. 225

Jones A., Noll S., Kausch W., Szyszka C., Kimeswenger S., 2013, A&A, 560, A91

Kornilov V. G., 2008, Astron. Rep., 52, 70

Kornilov V., 2014, J. Opt. Soc. America A, 31, 7

Kornilov V., Tokovinin A., Shatsky N., Voziakova O., Potanin S., Safonov B., 2007, MNRAS, 382, 1268

Kornilov V., Shatsky N., Voziakova O., Safonov B., Potanin S., Kornilov M., 2010, MNRAS, 408, 1233

Kornilov V., Sarazin M., Tokovinin A., Travouillon T., Voziakova O., 2012, A&A, 546, A41

Kornilov V. et al., 2014, PASP, 126, 482

Kornilov V. G. et al., 2016, Astron. Lett., 42, 616

Krisciunas K., 1997, PASP, 109, 1181

Leinert C., Vaisanen P., Mattila K., Lehtinen K., 1995, A&AS, 112, 99

Mattila K., Vaeisaenen P., Appen-Schnur G. F. O. V., 1996, A&AS, 119, 153
Mayer B., Kylling A., 2005, Atmos. Chemistry Phys., 5, 1855
Patat F., 2003, A&A, 400, 1183
Patat F., 2008, A&A, 481, 575
Pedani M., 2014, New Astron., 28, 63
Sánchez S. F., Aceituno J., Thiele U., Pérez-Ramírez D., Alves J., 2007, PASP, 119, 1186
Shettle E. P., 1990, Models of Aerosols, Clouds, and Precipitation for Atmospheric Propagation Studies, AGARD Conf. Proc. No. 454 on Atmospheric Propagation in the UV, Visible, IR, and MM-Wave Region and Related Systems Aspects
Tokovinin A., Kornilov V., 2007, MNRAS, 381, 1179
Tokovinin A., Kornilov V., Shatsky N., Voziakova O., 2003, MNRAS, 343, 891
van der A R. J., Allaart M. A. F., Eskes H. J., 2015, Atmos. Measurement Tech., 8, 3021
Voziakova O. V., 2012, Astron. Lett., 38, 271

This paper has been typeset from a TEX/LATEX file prepared by the author.